Global collisional gyrokinetic simulations of ITG microturbulence starting from a neoclassical equilibrium

2010 J. Phys.: Conf. Ser. 260 012021

(http://iopscience.iop.org/1742-6596/260/1/012021)

Journal of Physics: Conference Series **260** (2010) 012021 doi:10.1088/1742-6596/260/1/012021

Global collisional gyrokinetic simulations of ITG microturbulence starting from a neoclassical equilibrium

T Vernay[1], S Brunner[1], L Villard[1], B F McMillan[1], O Sauter[1], S Jolliet[2], T M Tran[1] and A Bottino[3]

[1] Centre de Recherches en Physique des Plasmas, Ecole Polytechnique Fédérale de Lausanne, Association EURATOM – Confédération Suisse, CH-1015 Lausanne, Switzerland
[2] Japan Atomic Energy Agency, Higashi-Ueno 6-9-3, Taitou, Tokyo, 110-0015, Japan
[3] Max-Planck-Institut für Plasmaphysik, Boltzmannstrasse 2, EURATOM Association, D-85748 Garching, Germany

E-mail: thibaut.vernay@epfl.ch

Abstract. Linearized operators describing inter-species and like-species collisions have been discretized and implemented in the gyrokinetic Particle-In-Cell (PIC) code ORB5 [S. Jolliet, Comp. Phys. Comm. **177**, 409 (2007)] based on the delta-f approach. Simulation results for neoclassical transport are compared with both analytical predictions as well as results from other codes. This new version of ORB5 including collisional dynamics thus makes it possible to carry out simulations of microturbulence starting from a global neoclassical equilibrium including self-consistent electric fields. First results of ITG microturbulence simulations carried out in this way are presented. The issue of numerical noise, inherent to the PIC approach and further accentuated by the implementation of collisions in the delta-f scheme, is addressed. It is shown how a noise reduction scheme based on a coarse graining procedure [Y. Chen and S. E. Parker, Phys. Plasmas **14**, 082301 (2007)] ensures the physical relevance of such simulations. Furthermore, a novel delta-f algorithm is presented, which switches between a canonical and a local Maxwellian background for carrying out the collisonless and collisional dynamics respectively, and its advantages are discussed.

1. Introduction

Gyrokinetic codes are devoted to the study of microturbulence and resulting anomalous transport in magnetic fusion plasmas. In these hot, low density plasmas, collisional effects are a relatively slow process compared to the characteristic time scale (i.e. frequencies and growth rates) of the microinstabilities underlying the small scale turbulence. Collisions have thus often been neglected in gyrokinetic simulations under the rationale of both reduced complexity of the required algorithm and reduced numerical cost. There is indeed a computational price for implementing collisions into gyrokinetic codes, especially in the frame of the δf Particle-In-Cell (PIC) approach in the form of increased numerical noise [1]. Nonetheless, in order for such simulations to account for full realistic interactions between particles, collisions have to be considered, as they may lead to various important phenomena regarding turbulent transport (e.g. modified growth rates of instabilities, damping of zonal flows).

This paper shows how collision operators, combined with a noise reduction scheme [2], make it possible to reach a neoclassical equilibrium, with a low noise level, which is a sound basis for starting global gyrokinetic simulations of microturbulence. A suitable collisional δf algorithm for carrying out runs at low collisionality is proposed [3], which takes advantage of the collisionless stationary solutions of the gyrokinetic equation. It results in some reduction in the computational cost of the simulation and thus provides a practical way to get relevant results related to collisional microturbulence.

The paper is organized as follows: Sec. 2 briefly presents the simulation model of the global gyrokinetic code ORB5 [4] including collisions. Sec. 3 describes the numerical methods used to solve the model. Sec. 4 shows some neoclassical benchmarks validating the collisional model. Sec. 5 proposes a novel algorithm for collisional gyrokinetic simulations switching between a local and a canonical Maxwellian background, for respectively carrying out the collisional and collisionless dynamics. This algorithm, combined with a noise reduction procedure, is then applied to global collisional gyrokinetic simulations of ITG microturbulence in Sec. 6. Conclusions are drawn in Sec. 7.

2. Simulation model

For the results presented in this paper, adiabatic electrons are assumed and the only kinetic species which is considered is Deuterium. In the frame of the gyrokinetic theory, f is the gyro-averaged particle distribution function. The distribution is usually expressed in terms of the gyrocenter variables $(\vec{R}, v_{||}, \mu)$, where $\vec{R}$ is the guiding centre position, $v_{||} = \vec{v}\cdot\vec{B}/B$ is the parallel velocity of the particle, $\vec{B}$ is the magnetic field and μ the magnetic moment. The gyrokinetic equation with collisions, governing the evolution of the ion distribution f, reads:

$$\frac{D}{Dt}f = -C(f), \tag{1}$$

where C is the ion self-collision operator and D/Dt is the collisionless gyrokinetic operator:

$$\frac{D}{Dt} = \frac{\partial}{\partial t} + \frac{\mathrm{d}\vec{R}}{\mathrm{d}t}\cdot\frac{\partial}{\partial\vec{R}} + \frac{\mathrm{d}v_{||}}{\mathrm{d}t}\frac{\partial}{\partial v_{||}}. \tag{2}$$

The time-derivatives of the gyrocenter variables $(\mathrm{d}\vec{R}/\mathrm{d}t, \mathrm{d}v_{||}/\mathrm{d}t, \mathrm{d}\mu/\mathrm{dt} = 0)$, implemented as particle trajectories in ORB5 [4], are given by the equations derived by Hahm [5]. The code uses a δf algorithm, where f is decomposed into a background f_0 and a perturbation δf: $f = f_0 + \delta f$. The background f_0 may be choosen as a local Maxwellian f_{LM} or a canonical Maxwellian f_{CM}. The self-collision operator appearing on the right hand side of Eq.(1) is linearized with respect to a local Maxwellian background: $C(f) \approx \hat{C}(\delta f_{LM})$ where $f = f_{LM} + \delta f_{LM}$, according to the procedure described in [1]. Moreover, the finite Larmor radius (FLR) effects are neglected in the collision operator, while they are retained in the collisionless dynamics for turbulence studies. The gyrokinetic equation for δf thus reads:

$$\frac{D}{Dt}\delta f = -\left[\frac{D}{Dt}f_0 + \hat{C}(\delta f_{LM})\right]. \tag{3}$$

The gyrokinetic equation is coupled with the quasi-neutrality relation, providing an equation for the self-consistent electrostatic potential ϕ:

$$\frac{en_{i0}(\Psi)}{T_e(\Psi)}[\phi(\vec{x},t) - \langle\phi\rangle(\Psi,t)] - \nabla_\perp\cdot\left(\frac{n_{i0}(\Psi)}{B\Omega_i}\nabla_\perp\phi\right) = \bar{\delta n}_i(\vec{x}), \tag{4}$$

where Ω_i is the ion cyclotron frequency, T_e is the electron temperature, e is the elementary charge and $\langle\rangle$ stands for the flux surface average operator. n_{i0} is the ion background density and $\bar{\delta n_i}$ is the perturbed gyrodensity contribution.

3. Numerical methods

Equation (3) is solved using the low-noise δf PIC method. N numerical particles, called markers, are introduced. They follow trajectories according to the gyrocenter equations [5]. In addition to phase space coordinates, each marker r has two so-called weights w_r and p_r [6], which are also functions of time and represent the fraction of the physical distributions δf and f_0, respectively, carried by each marker. The distribution functions f_0 and δf in gyrocenter variables are thus written as follows:

$$\delta f(\vec{R}, v_{||}, \mu, t) = \sum_r w_r(t)\delta[\vec{R} - \vec{R}_r(t)]\delta[v_{||} - v_{||,r}(t)]\delta[\mu - \mu_r(t)], \quad (5)$$

$$f_0(\vec{R}, v_{||}, \mu, t) = \sum_r p_r(t)\delta[\vec{R} - \vec{R}_r(t)]\delta[v_{||} - v_{||,r}(t)]\delta[\mu - \mu_r(t)]. \quad (6)$$

Evolving the gyrokinetic equation is thus performed by integrating numerically in time the marker trajectories together with weight equations. The toroidal angle φ and the square root of the normalized poloidal magnetic flux $s = \sqrt{\Psi/\Psi_{\text{edge}}}$ are used respectively as the toroidal and the radial coordinate. The poloidal coordinate is the straight-field-line angle θ^*, such that $\mathrm{d}\varphi/\mathrm{d}\theta^* = q_s = $ constant along a field line, with $q_s(\Psi)$ the safety factor on the magnetic surface $\Psi =$ constant. Collision operators, representing a diffusion process, add to the collisionless scheme random kicks in velocity space as well as modifications to the weight equations in order for the collisional algorithm to conserve particle number, parallel momentum and kinetic energy [7], [1]. The quasi-neutrality equation is solved in toroidal and poloidal Fourier spaces using a finite-element method [8]. The energy conservation of the code has been extensively tested [4].

4. Neoclassical benchmark

In order to test the implementation of the self-collision operator, the results presented in this section benchmark ion neoclassical transport obtained with ORB5 against analytical results, as well as previous numerical results from the drift-kinetic PIC code FORTEC-3D and the gyrokinetic Eulerian code GT5D [9]. The benchmark parameters are described in Tab. 1, with density and temperature profiles peaked at $r = 0.5a$. R_0 is the major radius, a the minor radius, T_e and T_i the electron and ion temperature respectively, $L_{Ti} = T_i/\nabla T_i$ and $L_n = n/\nabla n$ the characteristic lengths of the temperature and density gradient respectively at $r = 0.5a$. One defines $\rho^* = \rho_s/a$, where $\rho_s = c_s/\Omega_i$ is the sound Larmor radius for ions. The collisionality parameter ν^* is defined as the ratio between the detrapping collision frequency and the bounce frequency:

$$\nu^* = \frac{R_0 q_s}{\tau_{ii} v_{thi} \epsilon^{3/2}}, \text{ with } \tau_{ii} = \frac{6\sqrt{\pi}}{\nu_{ii}}, \quad (7)$$

where ν_{ii} is the ion-ion collision frequency, q_s is the safety factor and $\epsilon = r/R_0$ the local inverse aspect ratio. Figure 1 shows a collisionality scan for both the ion heat diffusivity χ_{Hi} and the coefficient k appearing in the neoclassical force balance relation (Eq.(20) in Ref. [9]). The heat diffusivity is given in units of $\chi_{GB} a/L_n$, where $\chi_{GB} = \rho_s^2 c_s/a$ is the Gyro-Bohm diffusivity. Analytical values of the heat diffusivity derived in the limit of large aspect ratio by Chang and Hinton (C-H) [10] are plotted as well. Predictions from the moment equation approach by Hirshman and Sigmar (H-S) [11] are shown in addition to results derived by Hinton and

$a/R_0 = 0.2$	$T_e/T_i = 1$	$R_0/L_{Ti} = 6$	$R_0/L_n = 6$	$1/\rho^* = 150$

Table 1. Run parameters, ion neoclassical transport benchmark

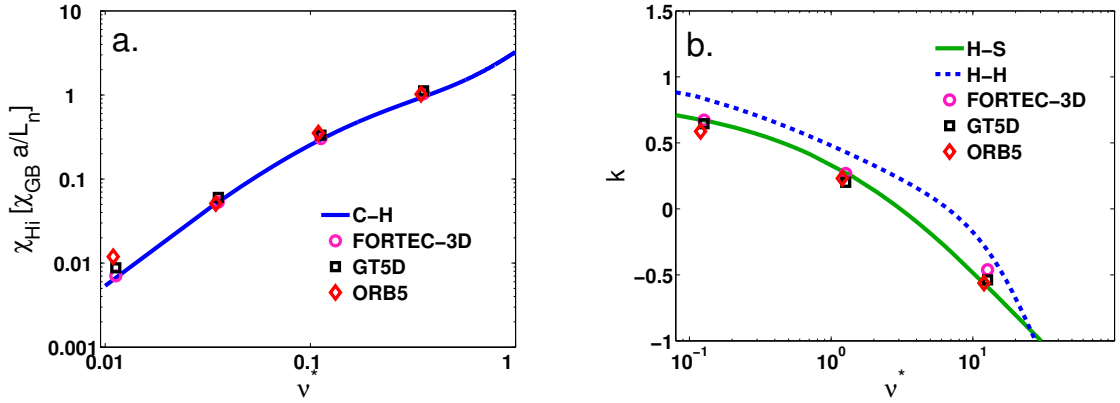

Figure 1. Considering parameters of Table 1. a) Ion heat diffusivity χ_{Hi} and b) neoclassical force balance coefficient k as a function of the effective collisionality. ORB5 results, shown for position $r/a = 0.5$ and at time $t \sim \tau_{ii}(r/a = 0.5)$, are compared to simulations from GT5D and FORTEC-3D, as well as analytical results from Chang and Hinton (C-H), Hinton and Hazeltine (H-H), Hirshman and Sigmar (H-S).

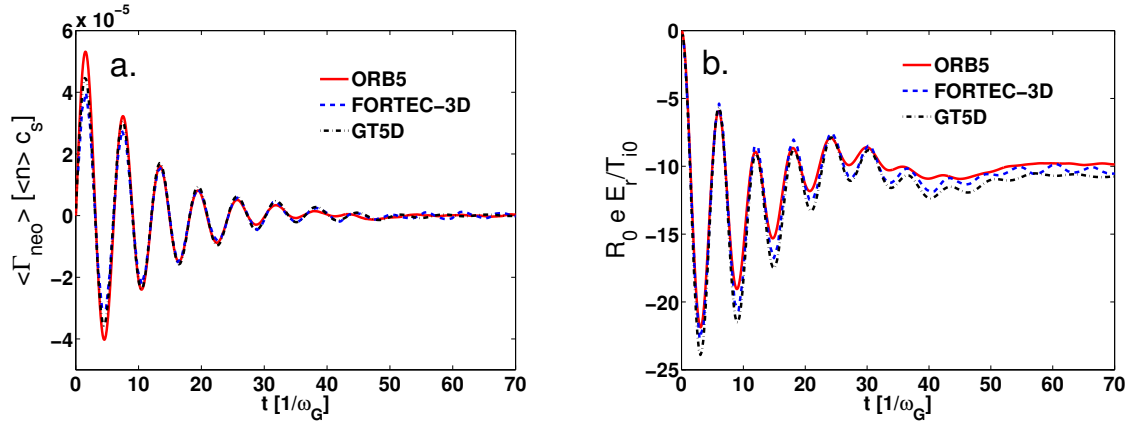

Figure 2. Time evolutions of a) ion gyrocenter flux Γ and b) radial electric field $E_r = -\partial\langle\phi\rangle/\partial r$ at $r = 0.5a$. Comparisons between results from ORB5, GT5D and FORTEC-3D. The ambipolarity is satisfied and an equilibrium neoclassical electric field is established. $\nu^*(r/a = 0.5) = 0.12$. ω_G is the GAM frequency.

Hazeltine (H-H) [12] for the coefficient k. The ambipolarity condition, i.e. a vanishing ion flux since the electrons are adiabatic, is verified in Figure 2.a, showing the time evolution of the ion gyrocenter flux at $r = 0.5a$. The setting up of the neoclassical radial electric field at $r = 0.5a$ is shown in Figure 2.b. The agreement between ORB5 results and those described in [9] is clearly very satisfactory.

5. Collisional δf-scheme with local/canonical Maxwellian background switching

The collisionless version of ORB5 usually makes use of a canonical Maxwellian (CM) background, which is a stationary state of the gyrokinetic equation:

$$f_{CM} = \frac{\mathcal{N}(\Psi_0)}{(2\pi\mathcal{T}(\Psi_0)/m)^{3/2}} \exp\left[-\frac{mv_{||}^2}{2\mathcal{T}(\Psi_0)} - \frac{B\mu}{\mathcal{T}(\Psi_0)}\right], \tag{8}$$

where "temperature" $\mathcal{T}$ and "density" $\mathcal{N}$ are functions of the toroidal canonical momentum $\Psi_0 = \Psi + qF(\Psi)v_{||}/mB$, where $F(\Psi) = RB_\varphi$ is the poloidal current flux function. At low collisionality, the full distribution f is still expected to be close to f_{CM}. Further considering f_{CM} as a background in this case thus appears advantageous as it enables to minimize the deviation δf and associated noise in the PIC representation. The self-collision operator is however naturally linearized with respect to a local Maxwellian (LM) background:

$$f_{LM} = \frac{n_0(\Psi)}{(2\pi T_0(\Psi)/m)^{3/2}} \exp\left[-\frac{mv_{||}^2}{2T_0(\Psi)} - \frac{B\mu}{T_0(\Psi)}\right], \tag{9}$$

where temperature and density are functions of the poloidal magnetic flux Ψ. In the frame of the two-weight scheme, it is possible to take advantage of the collisionless equilibrium function even in collisional runs, by performing a transformation from a canonical to a local background for carrying out the collisional step [3]. This transformation is based on the conservation of the total weight for each marker in both δf-representations (CM and LM):

$$f = f_{CM} + \delta f_{CM} = f_{LM} + \delta f_{LM} \tag{10}$$

$$\Longrightarrow \quad w_{CM} + p_{CM} = w_{LM} + p_{LM}. \tag{11}$$

A second equation required for the transformation is provided by the ratio σ of the p_{CM} and p_{LM} weights, which can be related to the ratio of the corresponding backgrounds:

$$\sigma = \frac{p_{CM}}{p_{LM}} = \left.\frac{f_{CM}}{f_{LM}}\right|_z, \tag{12}$$

where z is the position of the marker in phase-space. Before the self-collision algorithm, the local weights (w_{LM}, p_{LM}) are thus computed from the canonical weights (w_{CM}, p_{CM}) using Eqs. (11) and (12):

$$p_{LM} = \frac{p_{CM}}{\sigma}, \tag{13}$$

$$w_{LM} = w_{CM} + \left(1 - \frac{1}{\sigma}\right) p_{CM}. \tag{14}$$

The self-collisions are then carried out in the frame of the LM representation, computing in particular new positions in phase space z^* as well as modifications of the weights w^*_{LM} and p^*_{LM} as described in [1]. A new ratio $\sigma^* = f_{CM}/f_{LM}|_{z*}$ is then computed. Transforming back to the CM representation, using the inverse of relations (11) and (12), one obtains the collisional modified weights (w^*_{CM}, p^*_{CM}) in the CM representation and the code is ready for the next collisionless step, which uses again a canonical background. The scheme of the algorithm is described in Figure 3.

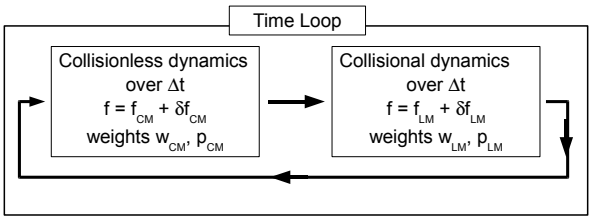

Figure 3. Mixed background collisional δf algorithm: Time loop for switching between a canonical Maxwellian background for stepping the collisionless dynamics and a local Maxwellian background for stepping the collisional dynamics.

6. Global collisional gyrokinetic simulations

The CYCLONE base case [13] is chosen in order to study the effects of the ion-ion self-collisions on ITG microturbulence, considering adiabatic electrons. The total initial distribution is a canonical Maxwellian, $f(t=0) = f_{CM}$, which is a stationary state of the collisionless gyrokinetic equation. Without collisions, simulations must start with a small perturbation to that equilibrium, in order for the turbulence to grow. With collisions, and at first enforcing axisymmetry by retaining only the toroidal Fourier mode $n = 0$, the full distribution will evolve towards a different distribution, i.e. a true neoclassical equilibrium together with the corresponding self-consistent axisymmetric electric field. After the neoclassical equilibrium has been reached, turbulence is switched on by letting the non-axisymmetric modes ($n \neq 0$) evolve freely. For the turbulent simulations, only every fourth toroidal Fourier mode is retained, namely $n = 0, 4, 8, \ldots, 56$, corresponding in real space to $1/4$ toroidal wedge. 500 million markers are used along with the following grid in configuration space for solving the quasi-neutrality relation: 128 points in the radial direction, 512 points in the poloidal direction and 256 points in the toroidal direction. These numerical parameters yield an average of ~ 30 markers per cell. However, since the quasi-neutrality equation is solved in poloidal and toroidal Fourier spaces, the important ratio is the number of markers per Fourier mode [14]. Invoking the alignment of microturbulence with the magnetic field lines, only the poloidal modes $m \in [nq_s - 5, nq_s + 5]$ are retained for each toroidal mode n. This filter leads to ~ 3 million markers per Fourier mode. It has been verified that even with collisions this resolution ensures converged results.

For the sake of clarity, the turbulent contribution to the energy flux Q_{turb} is defined as follows:

$$Q_{turb} = \left\langle \frac{\vec{\nabla} r}{|\vec{\nabla} r|} \cdot \int \mathrm{d}^3 v \frac{M v^2}{2} (f_0 + \delta f) \vec{v}_{E\times B} \right\rangle_S , \tag{15}$$

even though this term may contain a small neoclassical contribution, through the poloidally asymmetric modes ($n = 0, m \neq 0$). $\langle\rangle_S$ is the flux surface average operator and M the ion mass. The neoclassical contribution is defined as:

$$Q_{neo} = \left\langle \frac{\vec{\nabla} r}{|\vec{\nabla} r|} \cdot \int \mathrm{d}^3 v \frac{M v^2}{2} \delta f (\vec{v}_{\nabla B} + \vec{v}_c) \right\rangle_S , \tag{16}$$

where $\vec{v}_{\nabla B}$ is the ∇B drift and $\vec{v}_c$ the curvature drift. The simulation system considered has no heat sources, so that the temperature profile is free to relax towards marginally stable gradients with respect to the instabilities underlying the microturbulence. Figure 4.a shows the initial and

relaxed temperature profiles for both a collisionless case and for $\nu^*(r/a = 0.5) = 0.18$, which corresponds to a collisionality about 4.5 times larger than the one derived from the actual DIII-D parameters underlying the CYCLONE case. Let us point out that, in the collisional case, the system never fully relaxes, since the neoclassical heat transport persists even after the turbulent transport has vanished. As shown below and as expected, this neoclassical transport is however small compared to the fully developed turbulent transport in the first phase of the simulation, so that it is therefore appropriate to define the system as having reached a quasi-equilibrium state once the turbulent transport falls to the level of the neoclassical one. Figure 4.b shows the evolution of the ion heat diffusivity χ_{Hi} with respect to the effective ion temperature gradient R_0/L_{Ti}, averaged between $r = 0.3a$ and $r = 0.45a$. The critical gradient $R_0/L_{T\mathrm{crit}}$ is defined as the temperature gradient of the system once it has reached the quasi-equilibrium state as just defined. As clearly seen from Figures 4.a and 4.b, the critical gradient of the collisional case is lower than the critical gradient of the collisionless case. Indeed, collisions yield a critical gradient close to the linear stability of the most unstable ITG modes, $R_0/L_{Ti} \approx 5$. This is consistent with the fact that collisions damp the zonal flows and thus reduce the so-called Dimits shift, defined as the difference between the critical gradient for linear stability and the critical gradient observed in nonlinear collisionless gyrokinetic turbulent simulations. The latter is larger due to the stabilizing effect of zonal flows. By damping the zonal flows, ion-ion collisions thus increase the level of ITG turbulent heat transport, as has already been observed and discussed in Ref. [15].

The time evolution of the energy flux at $r = 0.5a$ is plotted in Figure 5.a, for the same cases. For the collisional simulation, the neoclassical phase (keeping only $n = 0$ modes) is carried out up to time $t = 2\tau_{ii}$, after which the turbulent phase is initiated (keeping modes $n \neq 0$ as well). The small discrepancy between the total flux and the $\vec{v}_{\nabla B} + \vec{v}_c$ contribution in the neoclassical phase is due to the small inward neoclassical $\vec{v}_{E\times B}$ contribution through the poloidally asymmetric modes, as explained above. The fully developed turbulent transport, corresponding to the bursty phase, is clearly much larger than the neoclassical transport. The neoclassical flux nevertheless becomes dominant once the temperature profile has relaxed. Figure 5.b presents the time evolution of the signal/noise ratio. The standard way of evaluating the noise in ORB5 has been described in Ref. [16]. The basic idea is to define the signal as the modes in a field-aligned Fourier filter, while the noise is made by the modes outside the Fourier filter. The considered runs made use of the coarse graining procedure [2]. Note that even in the late phase of the collisional simulation, the ratio remains above the threshold (considered to be of order ~ 10, see Ref. [16]) under which the predicted transport level is not relevant. As expected, with the same numerical parameters the collisionless simulation remains significantly less noisy.

7. Conclusions

Collisional effects have been added to the global gyrokinetic δf Particle-In-Cell code ORB5. Some benchmarks against analytical predictions and results from other codes have been performed, showing very good agreement and validating the implementation of the collision operators. A novel δf-algorithm, which switches between a canonical and a local Maxwellian background for respectively carrying out the collisionless and collisional dynamics in the frame of a time splitting scheme, has been presented. Starting from global neoclassical equilibria, preliminary results concerning collisional ITG microturbulence have been obtained and compared to collisionless runs. The nonlinear upshifted critical gradient appears to be reduced by the effect of ion-ion collisions. The crucial issue of numerical noise for PIC codes has

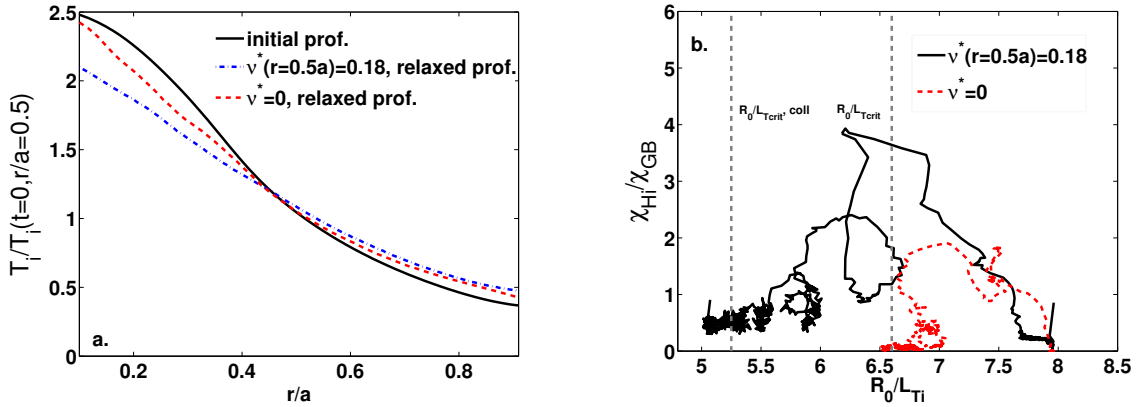

Figure 4. Collisionless and collisional turbulent CYCLONE case: a) Relaxation of the temperature profile towards the quasi-stationary state for both a collisionless and a collisional simulation. b) Evolution of the ion heat diffusivity $\chi_{Hi} = (Q_{neo} + Q_{turb})/(n_i|\nabla T_i|)$ in Gyro-Bohm units versus the temperature gradient. Collisions yield a lower nonlinear critical gradient. The quasi-stationary state is obtained when the heat diffusivity reaches the neoclassical level.

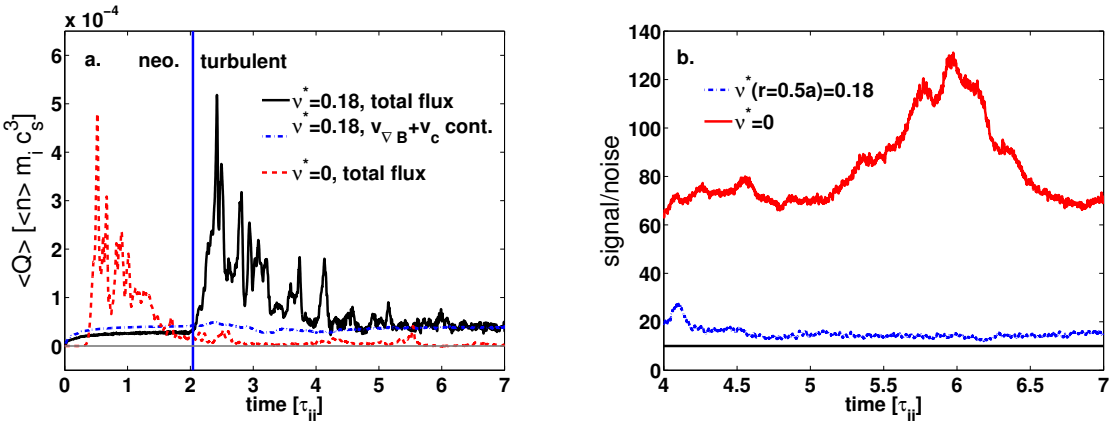

Figure 5. a) Time evolution of the total energy flux Q at $r/a = 0.5$ for both collisional (full line) and collisionless (dashed) simulations. Also shown is the neoclassical contribution for the collisional case (dash-dotted). In the bursty phase, the turbulent transport is much larger than the neoclassical transport. b) Signal/noise ratio for simulations using 500 million markers and coarse graining. The collisionless case is naturally less noisy, but the coarse graining enables to keep the collisional simulation above the relevance threshold ~ 10 even at later simulation times.

been adressed through the use of a coarse graining procedure, which enables high signal/noise ratios to be reached even in the turbulent phase of the simulation. These preliminary results open interesting perspectives for further work, especially the possibility to study collisional ITG microturbulence in presence of heat sources. The role of the FLR effects in ion-ion collision operator has also to be clarified. Finally, the study of collisional TEM microturbulence using kinetic electrons would be a challenging issue, taking account of the massive computer ressources it requires for getting physically relevant results.

Acknowledgements
Simulations were performed on the Monte Rosa CRAY XT-5 supercomputer of the Swiss National Supercomputing Center and the HPC-FF cluster of the Jülich Forschungszentrum. This work was partly supported by the Swiss National Science Foundation. The authors would like to thank S. Satake and Y. Idomura for supporting the benchmarking efforts by providing their own neoclassical data.

References

[1] Brunner S, Valeo E and Krommes J A 1999 *Physics of Plasmas* **6** 4504–4521
[2] Chen Y and Parker S E 2007 *Physics of Plasmas* **14** 082301
[3] Vernay T, Brunner S, Villard L, McMillan B F, Jolliet S, Tran T M, Bottino A and Graves J P 2010 *Physics of Plasmas* **17** 122301
[4] Jolliet S, Bottino A, Angelino P, Hatzky R, Tran T, McMillan B, Sauter O, Appert K, Idomura Y and Villard L 2007 *Computer Physics Communications* **177** 409 – 425
[5] Hahm T S 1988 *Physics of Fluids* **31** 2670–2673
[6] Hu G and Krommes J A 1994 *Physics of Plasmas* **1** 863–874
[7] Lin Z, Tang W M and Lee W W 1995 *Physics of Plasmas* **2** 2975–2988
[8] McMillan B, Jolliet S, Bottino A, Angelino P, Tran T and Villard L 2010 *Computer Physics Communications* **181** 715 – 719
[9] Satake S, Idomura Y, Sugama H and Watanabe T H 2010 *Computer Physics Communications* **181** 1069–1076
[10] Chang C S and Hinton F L 1982 *Physics of Fluids* **25** 1493–1494
[11] Hirshman S P and Sigmar D J 1981 *Nuclear Fusion* **21** 001079
[12] Hinton F L and Hazeltine R D 1976 *Rev. Mod. Phys.* **48** 239–308
[13] Dimits A M, Bateman G, Beer M A, Cohen B I, Dorland W, Hammett G W, Kim C, Kinsey J E, Kotschenreuther M, Kritz A H, Lao L L, Mandrekas J, Nevins W M, Parker S E, Redd A J, Shumaker D E, Sydora R and Weiland J 2000 *Physics of Plasmas* **7** 969–983
[14] Jolliet S 2009 Ph.D. thesis Ecole polytechnique fédérale de Lausanne
[15] Lin Z, Hahm T S, Lee W W, Tang W M and Diamond P H 1999 *Phys. Rev. Lett.* **83** 3645–3648
[16] Bottino A, Peeters A G, Hatzky R, Jolliet S, McMillan B F, Tran T M and Villard L 2007 *Physics of Plasmas* **14** 010701